Supplemental Tables

Table S1. Comparison of technologies. Related to Figure 1.

Technology	Spatially resolved	Transcriptome resolution	Transcriptome coverage	TCR sequences	Notes
Single-cell TCR sequencing	No	Single cell	Whole transcriptome	V(D)J, CDR3	E.g., 10X Chromium Single Cell V(D)J.
Laser capture microdissection	Yes[56,57]	10 - 1000 cells	Whole transcriptome	V(D)J, CDR3	
Fluorescence in situ hybridization	Yes	< 1 µm	Limited	Need to know sequences a priori	E.g., MERFISH[58], SeqFISH+[59], RNAScope.
Tetramer-based cytometry	No	Single cell	None	Need to know antigen & epitope a priori	E.g., flow cytometry sorting with sequencing; mass cytometry (109 epitopes[60])
Spatial barcoding with capture of mRNA	Yes	55 - 110 µm	Whole transcriptome	None	E.g., 10X Visium
In situ sequencing	Yes	< 1 µm	Limited	None	E.g., ISS (30 bases)[61]
Spatial barcoding with capture of mRNA & TCR sequencing	Yes[62]	55 - 110 µm	Whole transcriptome		

Slide-TCR-seq	Yes	10 µm	Whole transcriptome	V(D)J, CDR3	

Supplemental Figures

A

All samples | Human | Mouse

Number of Beads with TCRs

Miseq / Nanopore

Sequencing method

B

Miseq log10(fraction of clones) vs Nanopore log10(fraction of clones)

R=0.81

C

B | CD4 T | MP

Memory T | CD8 T | NK

D

B | CD8 T | CD4 T | CD4 MP | CD8 MP

Memory T | Activated MP | NK

E

Beads with Constant: 8777 | 6277 | 2525 Beads with variable

41.7% (6277/15,054) | 71.3% (6277/8802)

F

UMIs count

H

variable UMIs vs constant UMIs

r = 0.86

G

UMIs count

Figure S1. Benchmarking Slide-TCR-seq sequencing and OT-I mouse spleen clonotype pairing and cell-type mapping. Related to Figure 1.

(A) Comparing the number of beads with TCRs detected in Nanopore long-read sequencing and MiSeq short-read sequencing across human renal cell carcinoma and OT-I mouse spleen samples. Barplots indicate means, and error bars indicate the standard deviation of replicates. We hypothesize that the improvement with Nanopore sequencing is in part due to human alpha and beta sequences being longer (~1300 nt and ~1100 nt) than the mouse OT-I sequences (~1000 nt), making it slightly harder for the human sequences to cluster on the MiSeq. As the MiSeq has a lower error rate, when the sequences do cluster, mouse TCR sequences sequenced on the MiSeq outperform those sequenced via Nanopore.

(B) Correlation between the fraction of each TCR in four pucks of renal cell carcinoma when sequenced by Nanopore long-read sequencing and MiSeq short-read sequencing (R=0.81).

(C) RCTD-assigned cell types for spleen plotted individually from the same array.

(D) Frequency of cell-type assignments as identified by RCTD.

(E) Frequency of TCR constant and variable sequences detected on the same bead.

(F) Spatial heatmap of beads with at least one read of *Trac* or *Trbc2* constant sequence (bin size = 50 pixels or 32.5 µm).

(G) Spatial heatmap of beads with at least one read of CDR3 variable sequence after computational filtering (bin size = 50 pixels or 32.5 µm).

(H) Correlation between spatial heatmaps of constant and variable TCR Unique Molecular Identifier (UMI) sequences in spleen (Pearson's r=0.86).

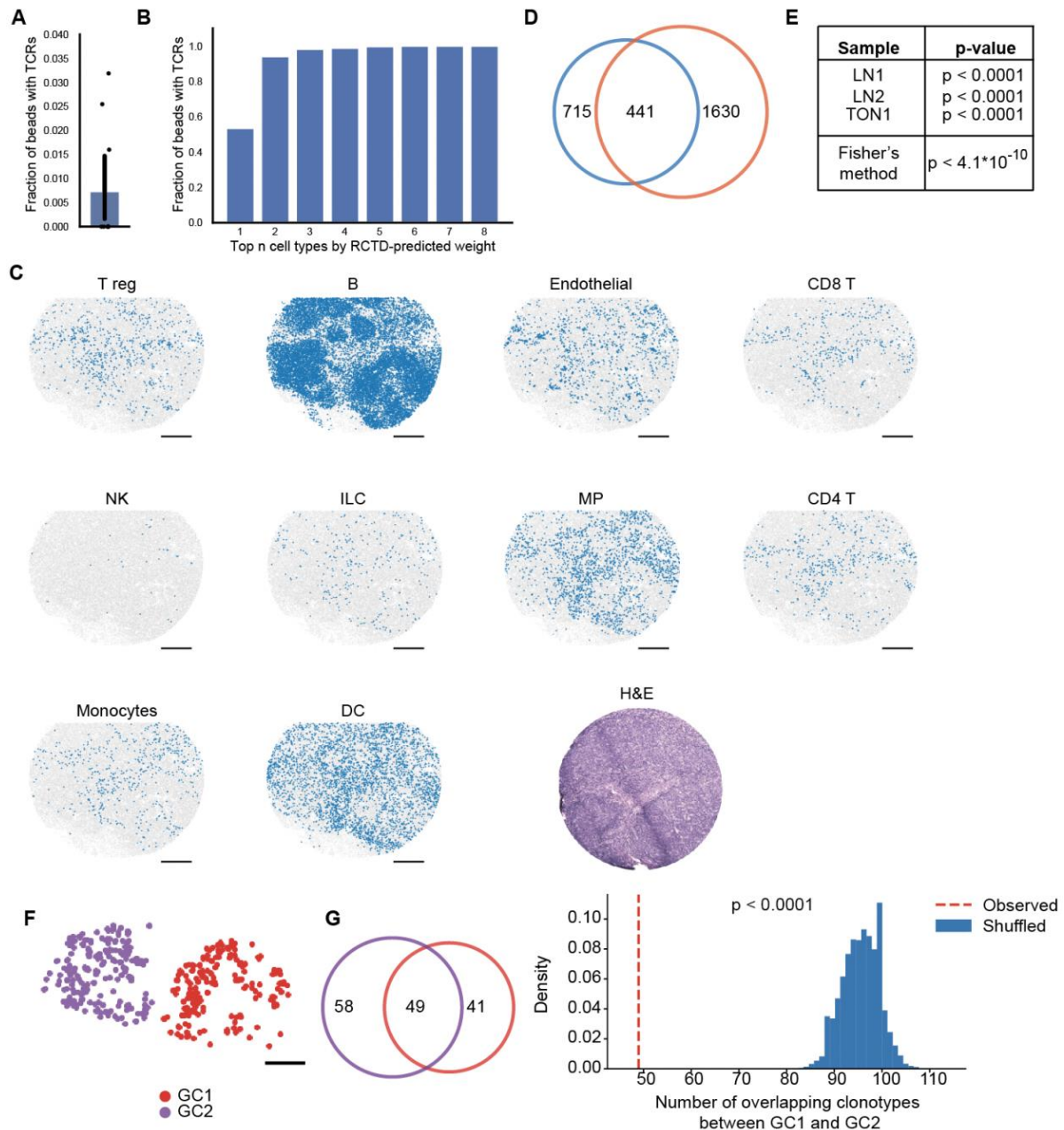MP = macrophage. NK = natural killer. All scale bars: 500 µm.

Figure S2. Slide-TCR-seq applied to lymph node and tonsil samples. Related to Figure 2.
(A) Fraction of beads with a TCR that have another bead within 15 μm with the same TCR in a lymph node array (n=10, bar plots indicate means, and error bars indicate standard deviation of replicates.)
(B) For beads containing TCRs, the fraction of beads predicted by RCTD to be T cells based on transcriptome data in a lymph node puck.
(C) RCTD-assigned cell types and hematoxylin and eosin stain for RCC plotted individually from the array in Figure 2A. During the initial indexing step for this puck, a section of beads was not imaged, resulting in a cutoff final shape.
(D) For all clonotypes, a Venn diagram showing the clonotype overlap between GC (blue) and non-GC (orange) regions in a reactive lymph node.

(E) Significance of the observed number of shared clonotypes between GCs compared to the expected number from randomly shuffled assignments for three secondary lymphoid organ samples. Combined p-value using Fisher's method.
(F) K-means clustering distinguishing two GCs in a serial section of a human reactive lymph node.
(G) (Left) For clonotypes detected on >1 bead, a Venn diagram showing clonotype overlap between GC1 (purple) and GC2 (red) regions. (Right) - The significance of the observed number of shared clonotypes between GCs compared to the expected number from randomly shuffled assignments.
All scale bars: 500 µm. LN = lymph node. TON = tonsil.

A Pre-treatment / Post-treatment

B, Tumor, Epithelial, Lung, Mast, Myeloid, NK, CD4 T, CD8 T, Treg

B Pre-treatment / Post-treatment

C B, Myeloid, CD4, CD8 T, Epithelial, Kidney, Lung, Tumor, Mast, NK, T reg

F Pre-treatment / Post-treatment

RCC1, RCC2, cycRCC

G Pearson's correlation / Tumor enrichment: Enriched, Depleted

D Cell type / Clonotype

E Cell type / Clonotype

H $r_P = 0.79$ $p = 9 \times 10^{-15}$

$\log_{10}$(Slide-TCR-seq fraction) vs $\log_{10}$(bulk TCR fraction)

I
Post-treatment 1 vs 2: $r_P = 0.45$ $p = 1 \times 10^{-7}$
Post-treatment 1 vs 3: $r_P = 0.44$ $p = 3 \times 10^{-7}$
Post-treatment 2 vs 3: $r_P = 0.42$ $p = 6 \times 10^{-6}$

$\log_{10}$(clonotype UMIs)

J CDF / Number of unique clonotypes / pre-treatment, post-treatment

K Bulk TCR-seq: pre-treatment 102, 54, 10698 post-treatment
Slide-TCR-seq: pre-treatment 31, 10, 1213 post-treatment

L
CASSPRGAYEQYF, CASSRGAASYNEQFF, CASSFRGSYEQYF, CASNLRGAGDNEQFF, CASSLETGTGELFF, CATSDSAGRNNEQFF, CASSHEAERIRDFYEQYF, CASSLEGYEQYF, CASSLDIRGYEQFF, CASSMGTAYEQYF

$\log_{10}$(Fraction in post-treatment) vs $\log_{10}$(Fraction in pre-treatment)

Higher in pre- than post-treatment
Higher in post- than pre-treatment

Figure S3. Spatial organization and clonotype analyses of pre- and post-treatment RCC. Related to Figure 3.

(A) Plot of all RCTD cell assignments for pre-treatment (top panel, n=2 replicate arrays) and post-treatment (bottom panel, n=3 replicate arrays) specimens.

(B) Plot of all clonotypes for pre-treatment (top panel, n=2 replicate arrays) and post-treatment (bottom panel, n=3 replicate arrays) specimens. Clonotype CDR3 sequences were queried in VDJdb (https://vdjdb.cdr3.net/) to identify any with known HLA-matched antigen specificity, among which only rare clonotypes (<3.5% of pre- and post-treatment clonotypes) were identified – the majority of which were annotated as anti-viral specificity and none of which met the criteria for inclusion in the T clonotype analyses.

(C) RCTD-assigned cell types for RCC plotted individually from the array in Figure 3B. Annotations are from a published RCC scRNA-seq dataset that included this patient's sample[22].

(D) The count of each TCR clonotype's beads within the tumor compartment that have at least one feature of interest bead in their 13 μm radius.

(E) Heatmap showing, per cell type row, the proportion of a TCR clonotype's beads that include at least one bead of that cell type within a 13 μm radius. Spatial interactions identified between TCR clones and microenvironmental cells in the post-ICB metastasis included the colocalization of TCR-26 clones with dendritic cells (p=0.008), TCR-10 clones with macrophages (p=0.006), and TCR-18 with fibroblasts (p=0.004). For all analyses, data were aggregated across the three post-ICB arrays, and clonotypes with at least 20 beads across three arrays were selected (n=26). Proportions were z-score normalized across each row. The number of tumor-compartment beads for each TCR and cell type is depicted along the top and left axes, respectively. Corresponding raw counts for the heatmap are shown in Figure S4D. Cells that reached significance (not corrected for multiple hypothesis testing, given our small sample size) were identified by p values *<0.05; **<0.01; ***<0.005.

(F) Within-tumor spatial localization of 3 distinct RCC cell subtypes across pre- and post-treatment arrays.

(G) Correlation between different clonotypes' non-negative matrix factorized cell loadings by Pearson's correlation.

(H) Comparing clonotype fractions for clonotypes with at least 10 counts in Slide-TCR-seq and bulk TCR sequencing of the post-treatment RCC specimen by Pearson's r.

(I) Comparing the consistency of UMI counts per clonotype, normalized by total TCR counts, between all three post-treatment arrays by Pearson's r.

(J) Cumulative distribution function (CDF) showing the diversity and abundance of the clonotypes in Slide-TCR-seq (top) and bulk TCR sequencing (bottom).

(K) Comparing the clonotypes in the pre-treatment and post-treatment specimens for bulk TCR (top) and Slide-TCR-seq (bottom).

(L) Showing the change in clonotype fraction for clonotypes that were shared in pre- and post-treatment in Slide-TCR-seq (left panel) and bulk TCR-seq (right panel; transparency alpha of dots was set at 0.3 to display density).

DC = dendritic cell, NK = natural killer, Treg = regulatory T cell.
All scale bars: 500 μm. Three distinct transcriptional profiles[52]: RCC1 (upregulated kidney morphogenesis and angiogenesis gene sets), RCC2 (upregulated metabolism programs), and cycRCC (upregulated cell cycle gene sets).
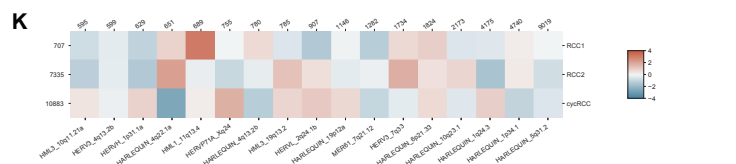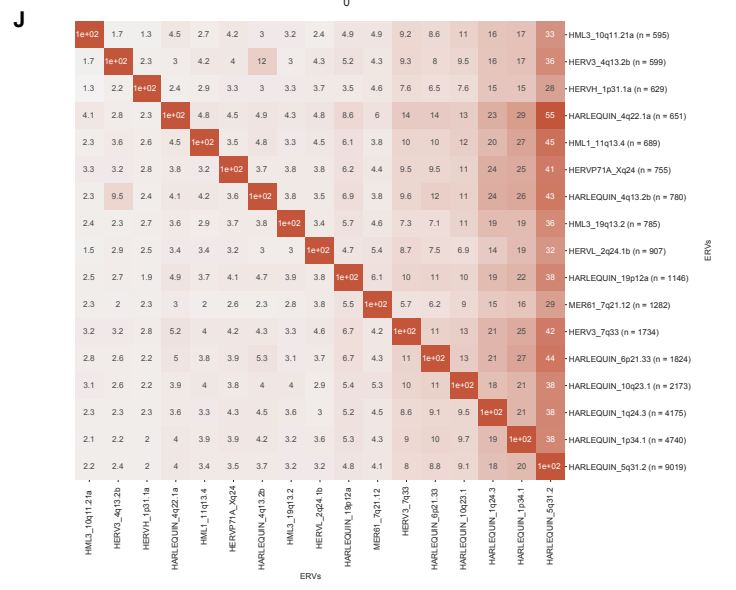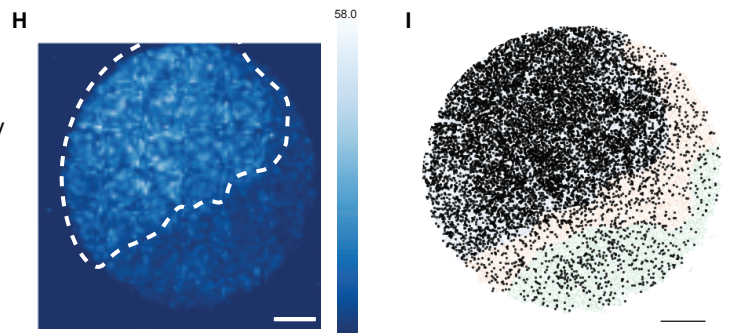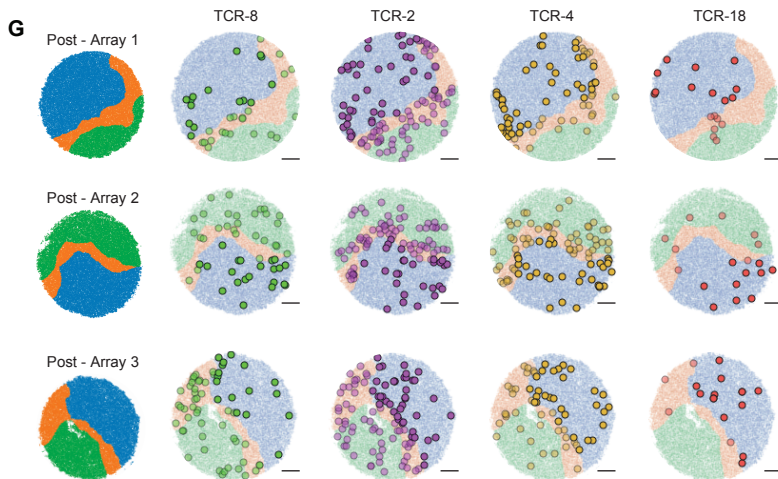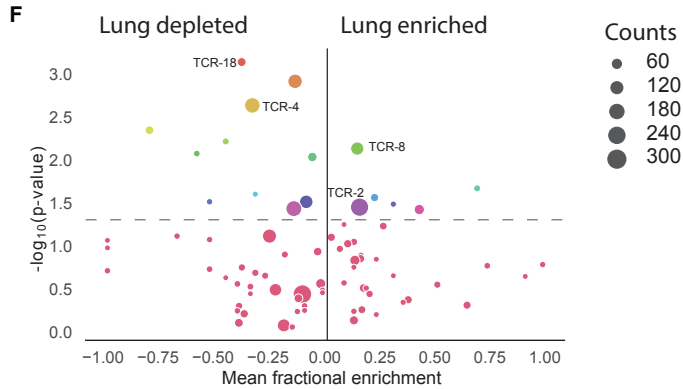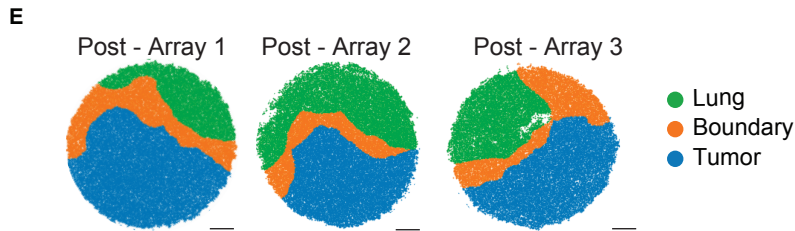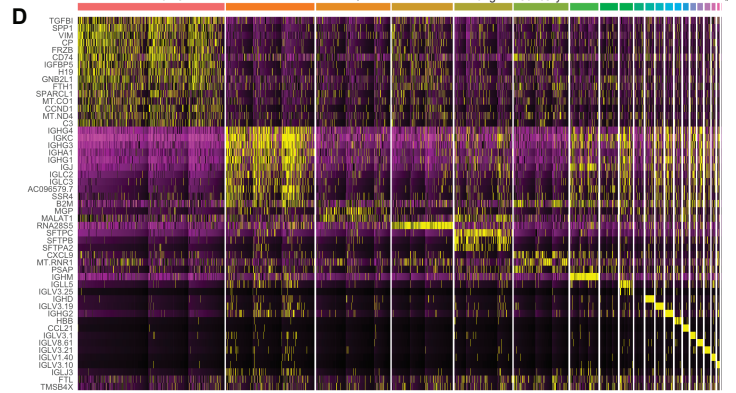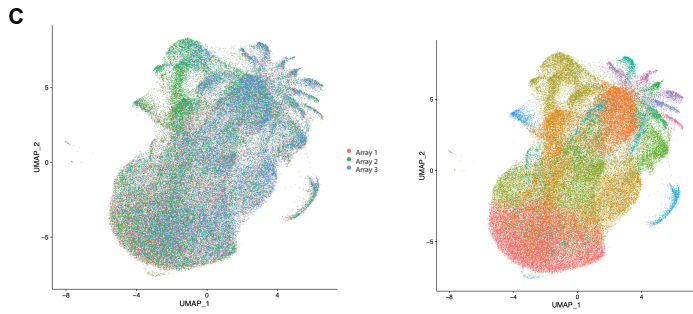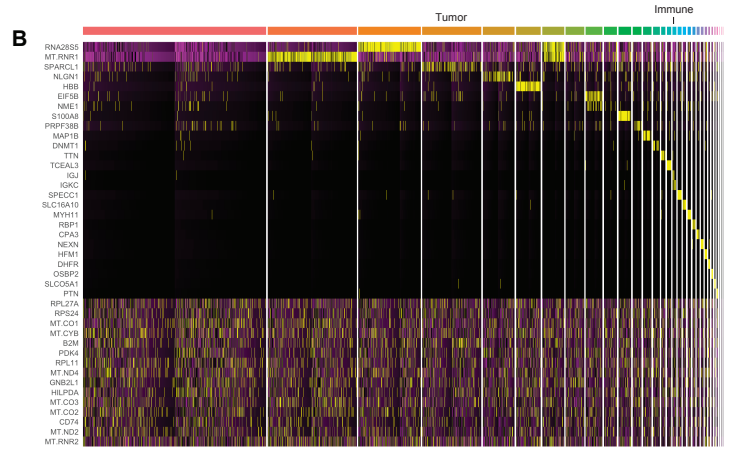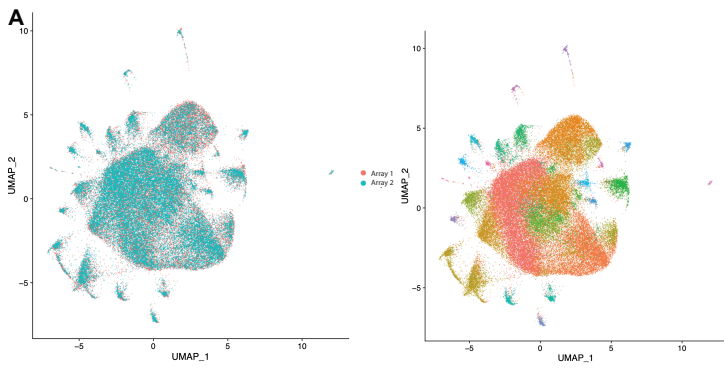
Figure S4. Cell compartment assignment using unsupervised clustering for analyzing differential tumor enrichment between clonotypes in the post-treatment RCC specimen and spatially probing endogenous retroviral (ERV) expression. Related to Figure 3.

(A) UMAP of co-clustered arrays for pre-treatment RCC specimen, colored by array (left panel) and by cell type clusters (right panel).

(B) Heatmap of markers for each pre-treatment RCC cell cluster.

(C) UMAP of co-clustered arrays for post-treatment RCC specimen, colored by array (left panel) and by cell type clusters (right panel).

(D) Heatmap of markers for each post-treatment RCC cell cluster.

(E) Cell compartment assignment for each array.

(F) Significance of clonotype spatial distributions compared against all other clonotypes from the post-treatment specimen plotted against lung enrichment (n=3 replicate arrays). Each color represents one clonotype. Grey dots indicate clonotypes that were not significantly enriched.

(G) Visualization of select clonotypes that are significantly enriched or depleted in the tumor compartment for each post-treatment array. T cells within the tumor compartment are displayed as opaque, and T cells within other compartments are shown as translucent.

(H) Gaussian-filtered heatmap for visualizing the spatial distribution of all ERV expression (in UMI counts) in the post-treatment RCC lung metastasis array from Figure 3B. ERV expression was identified using Telescope. Dashed line delineates the tumor compartment.

(I) Spatial localization of beads expressing the predominant HARLEQUIN ERV family (black dots).

(J) To assess the co-expression of ERVs in RCC cells, the frequency with which beads in the tumor compartment expressed each ERV was quantified. For each expressed ERV (y-axis), the percent of beads in the tumor region that also co-expressed another ERV (x-axis) was displayed using a heatmap. ERVs were included in the analysis if they were expressed by at least 500 tumor-compartment beads in the three post-treatment RCC arrays and expressed in less than %1 of non-tumor cells in matched scRNA-seq data from the pre-treatment sample, thereby excluding ERVs that demonstrated high expression in non-tumor cells.

(K) Z-score normalized proportions of ERV-expressing beads that were predicted to be one of three RCC subtypes by RCTD.
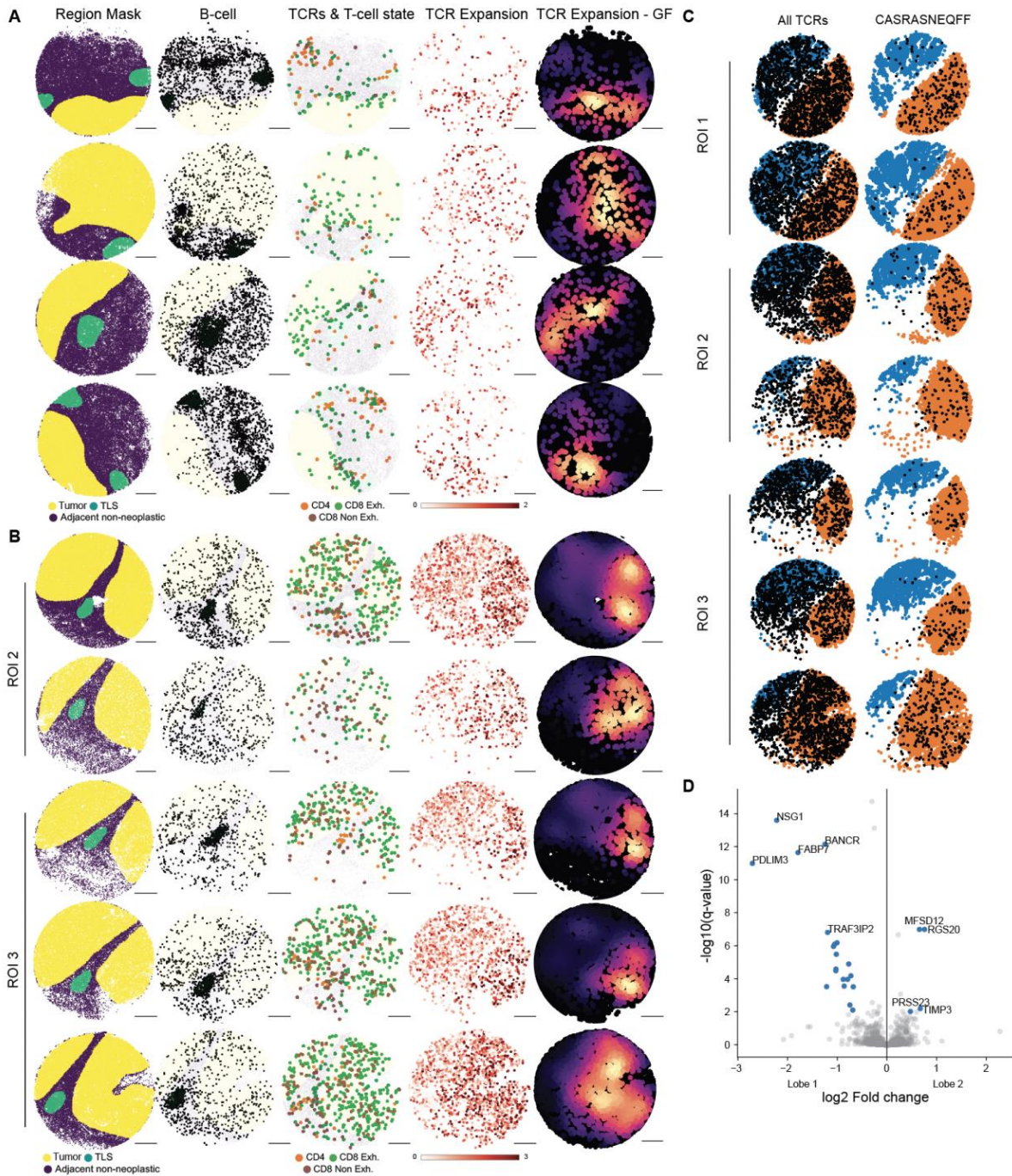
All scale bars: 500 µm.

Figure S5. T cell and tumor cell differences in renal cell carcinoma and melanoma. Related to Figures 4 and 5.

(A) All replicates of the renal cell carcinoma samples in Figures 4E and 4G. From left to right, 1 – a region mask of a Slide-TCR-seq array delineating tumor, TLS, and adjacent non-neoplastic regions. 2 – a plot of B cells identified through RCTD. 3 - beads containing both CDR3 and T cell state colored by RCTD assignment. 4 – beads containing CDR3 colored by log10(total number of T cells for that clone). 5 – Gaussian-filtered heatmap visualizing TCRs weighted by the extent of clonal expansion.

(B) All replicates of the melanoma samples in Figures 4F and 4H. From left to right, 1 – a region mask of a Slide-TCR-seq array delineating tumor, TLS, and adjacent non-neoplastic regions. 2 – a plot of B cells identified through RCTD. 3 - beads containing both CDR3 and T cell state colored by RCTD assignment. 4 – beads containing CDR3 colored by log10(total number of T cells for that clone). 5 – Gaussian-filtered heatmap visualizing TCRs weighted by the extent of clonal expansion.

(C) All replicates used in analyses in Figure 5. Visualization of all TCRs (left) and the CASRASNEQFF TCR clonotype (right) across all replicate arrays.

(D) Differentially expressed genes between tumor cells from the two distinct lobes of the metastatic melanoma, with blue dots representing statistically significant genes with absolute log fold change > 0.4.